PARTICLE PRECIPITATION INTO THE THERMOSPHERE
(Invited Review)

Patricia H. Reiff
Department of Space Physics and Astronomy
Rice University, Houston, TX 77251-1892

Particle precipitation plays an important role in thermospheric dynamics, often being both the most important ionization source and the most important heat source, comparable to Joule heating rates in the auroral zones [Harel et al., 1981; Rees, et al., 1983; see Reiff, 1983a] and typically exceeding solar ultraviolet as an ionization mechanism in the nightside auroral zones and winter polar caps (Figure 1, from Wallis and Budzinski, [1981]). Rees [1963] has shown that, roughly speaking, one electron-ion pair is produced by each 35 eV of incident electron energy flux; thus, over half of the incident electron energy flux goes into heating rather than into ionization. Precipitating ions also can produce ionization, also requiring roughly 35 eV per pair [Rees, 1982]; however, since ion energy fluxes are typically much weaker than electron fluxes, they have often been neglected.

The altitude at which the electrons and ions deposit their energy is strongly dependent on particle energy, with ionization occurring at progressively lower altitudes for increasingly more energetic electrons. For 300 keV electrons, the altitude of maximum ionization occurs at 72 km; 95 km for 40 keV; $\sim$107 km for 10 keV, $\sim$170 km for 1 keV, and $>$ 216 km for 0.4 keV [Figure 2, from Rees, 1963]. Ions deposit their energy at altitudes higher than electrons of comparable energy [Rees, 1982]. The altitude of ionization becomes important in determining resultant conductivity profiles, with lower altitudes favoring a higher ratio of Hall to Pedersen conductance; this in turn affects the height distribution of Joule heating rates.

The bulk of the particle precipitation occurs on field lines which map to the plasma sheet and ring current regions. The auroral zone precipitation is greatly enhanced over its typical loss cone fluxes by the existence of electric fields parallel to the magnetic field line [Knight, 1973]. The auroral electric fields are associated with upward field-aligned (Birkeland) currents. The lower-latitude ring current precipitation is caused principally by pitch-angle scattering in the equatorial plane. (See review by Reiff, [1983b]).

It is not currently possible (nor is it likely in the near future) to have a complete, detailed, global distribution of particle precipitation on a nearly-continuous basis, although progress is being made using several complementary techniques. In-situ spacecraft and rocket particle observations are extremely useful and yield results on very good spatial scales along the flight track (km to m, for rocket flights); global models, however, must be constructed statistically, and as such lose much small-scale detail (Figure 3, from Spiro et al. [1982]). Using a number of spacecraft (Tiros and DMSP), separated in local time, one can construct a global energy flux estimate with roughly 15-minute time resolution [David Evans, personal communication, 1984]; however, obtaining a two-dimensional pattern from combining different in-situ data sets is a cumbersome technique and cannot at present be done accurately with less than a two-hour time resolution [Simons et al.,

1985]. Some of the statistical models have become very detailed, however, with complete spectra (not just energy flux and average energy) available at each local time-latitude bin (Figure 4 from Hardy et al., [1985]). Incoherent radar studies can also be used to infer precipitating electron fluxes [Vondrak and Baron, 1977], but they also are limited in field of view.

Optical techniques show perhaps the most promise for developing an accurate two-dimensional pattern on reasonable time scales. Images from high altitude (such as Dynamics Explorer and the proposed International Solar Terrestrial Research Program) have the advantage of global coverage at ten-minute time resolution, at the expense of spatial resolution ($\sim$ 50 km) [Frank et al., 1982]. Lower-orbiting spacecraft, such as Hilat and DMSP (which will add ultraviolet imaging to its optical data starting in 1989), have much better spatial resolution ($\sim$ km); however, a single pass generally cannot image the entire auroral zone, and is repeated only with 45-minute time resolution (e.g., Meng and Huffman, 1984). Ultraviolet and X-ray imaging are particularly helpful, since they are responsive to the more energetic particles, and, combined with optical data, can yield a reasonable estimate of the energy distribution of the precipitating particles. [e.g., Luhmann, 1977; Imhof et al., 1982]. Calibration of the optical images by "ground truth" (images which include radar facilities) or "space truth" (in situ particle detectors) is vital and is currently underway.

In summary, the particle precipitation into the thermosphere is both an important ionization source and an important heat source; since the globally-integrated value can vary over more than a factor of ten, and the instantaneous local rate can vary over nearly three orders of magnitude (Figure 5, from Spiro et al., [1982]) global maps of precipiation rates are extremely important for predicting thermospheric "weather."

Acknowledgements

This work was supported by the Atmospheric Sciences Division of the National Science Foundation (grant ATM 83-06772), and by the National Aeronautics and Space Administration (grant NGR 44-006-137).

REFERENCES

Frank, L. A., J. D. Craven, J. C. Burch and J. D. Winningham, Polar views of the earth's aurora with Dynamics Explorer, *Geophys. Res. Lett., 9,* 1001-1004, 1982.

Hardy, D. A., M. S. Gussenhoven, and E. Holeman, A statistical model of auroral electron precipitation, *J. Geophys. Res.,* (in press), 1985.

Harel, M., R. A. Wolf, R. W. Spiro, P. H. Reiff, C. K. Chen, W. J. Burke, F. J. Rich and M. Smiddy, Quantitative simulation of a magnetospheric substorm. 2. Comparison with observations, *J. Geophys. Res., 86,* 2242-2260, 1981

Imhof, W. L., J. Stadsnes, J. R. Kilner, D. W. Datlowe, G. H. Nakano, J. B. Reagan, and P. Stauning, Mappings of energetic electron precipitation following substorms using the satellite bremsstrahlung technique, *J. Geophys. Res., 87,* 671-680, 1982.

Knight, S., Parallel electric fields, *Planet. Space Sci., 21,* 741-750, 1973.

Luhmann, J. G., Auroral bremsstrahlung spectra in the atmosphere, *J. Atmos. Terr. Phys., 39,* 595, 1977.

Meng, C. -I., and R. E. Huffman, Ultraviolet imaging from space of the aurora under full sunlight, *J. Geophys. Res., 11,* 315-318, 1984.

Rees, M. H., Auroral ionization and excitation by incident energetic electrons, *Planet Space Sci., 11,* 1209-1218, 1963.

Rees, M. H., On the interaction of auroral protons with the earth's atmosphere, *Planet. Space Sci., 30,* 463-472, 1982.

Rees, M. H., B. A. Emery, R. G. Roble, and K. Stamnes, Neutral and ion gas heating by auroral electron precipitation, *J. Geophys. Res., 88,* 6289-6300, 1983.

Reiff, P. H., Models of auroral zone conductances, in *Magnetospheric Currents,* ed. T. A. Potemra, p. 180-191, AGU Press, Washington, 1983a.

Reiff, P. H., Polar and auroral phenomena: A review of U.S. progress during 1979-1982, *Rev. Geophys. space Phys., 21,* 418-433, 1983b.

Simons, S. L., P. H. Reiff, R. W. Spiro, D. A. Hardy, and H. W. Kroehl, A comparison of precipitating electron energy flux on March 22, 1979 with an empirical model, *J. Geophys. Res.,* (in press), 1985.

Spiro, R. W., P. H. Reiff, and L. J. Maher, Jr., Precipitating electron energy flux and auroral zone conductances - an empirical model, *J. Geophys. Res., 87,* 8215-8227, 1982.

Vondrak, R. R. and M. J. Baron, A. method of obtaining the energy distribution of auroral electrons from incoherent scatter radar measurements, in *Radar Probings of the Auroral Plasma,* Proceedings of the EISCAT summer school, Tromso, Norway, 1975, ed. A. Brekke (Universitetforlaget, Tromso-Oslo-Bergen, 1977), p. 315-330.

Wallis, D. D., and E. E. Budzinski, Empirical models of height integrated conductivities. *J. Geophys Res., 86,* 125-137, 1981.

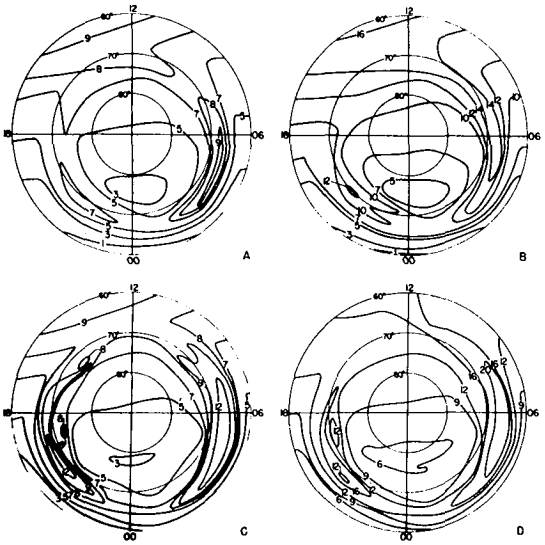

Figure 1. Contour plots of Σ_P and Σ_H (mhos) for the two K_p cases produced by particle, background, and solar sources for 1700 UT on April 1. (a) Σ_P for $0 \leq K_p \leq 3_0$, (b) Σ_H for $0 \leq K_p \leq 3_0$, (c) Σ_P for $3_0 < K_p$, (d) Σ_H for $3_0 < K_p$ [from Wallis and Budzinski, 1981].

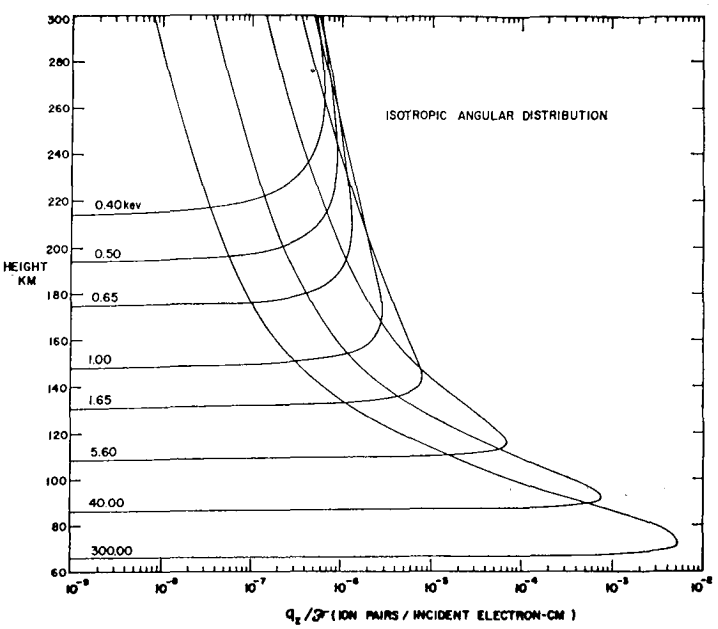

Figure 2. Ionization profiles for incident isotropic monoenergetic electrons of energies between 0.40 and 300 keV, respectively [from Rees, 1963].

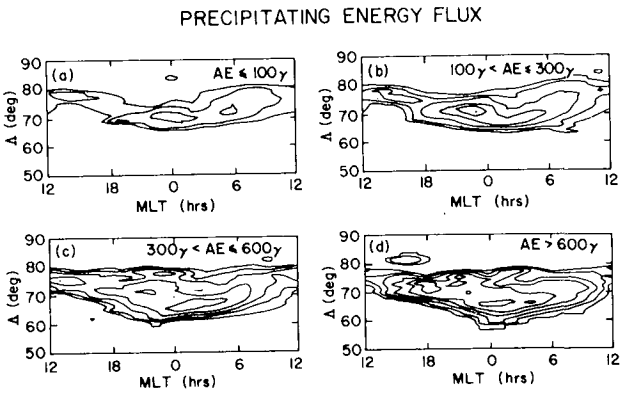

Figure 3. Contours of constant precipitating electron energy flux sorted according to auroral electrojet (AE) index. The outermost contours correspond to a bin-average energy flux of 2.5 x 10^{-1} erg cm^{-2} s^{-1}, with adjacent contours representing factor of 2 increases in energy flux [from Spiro et al., 1982].

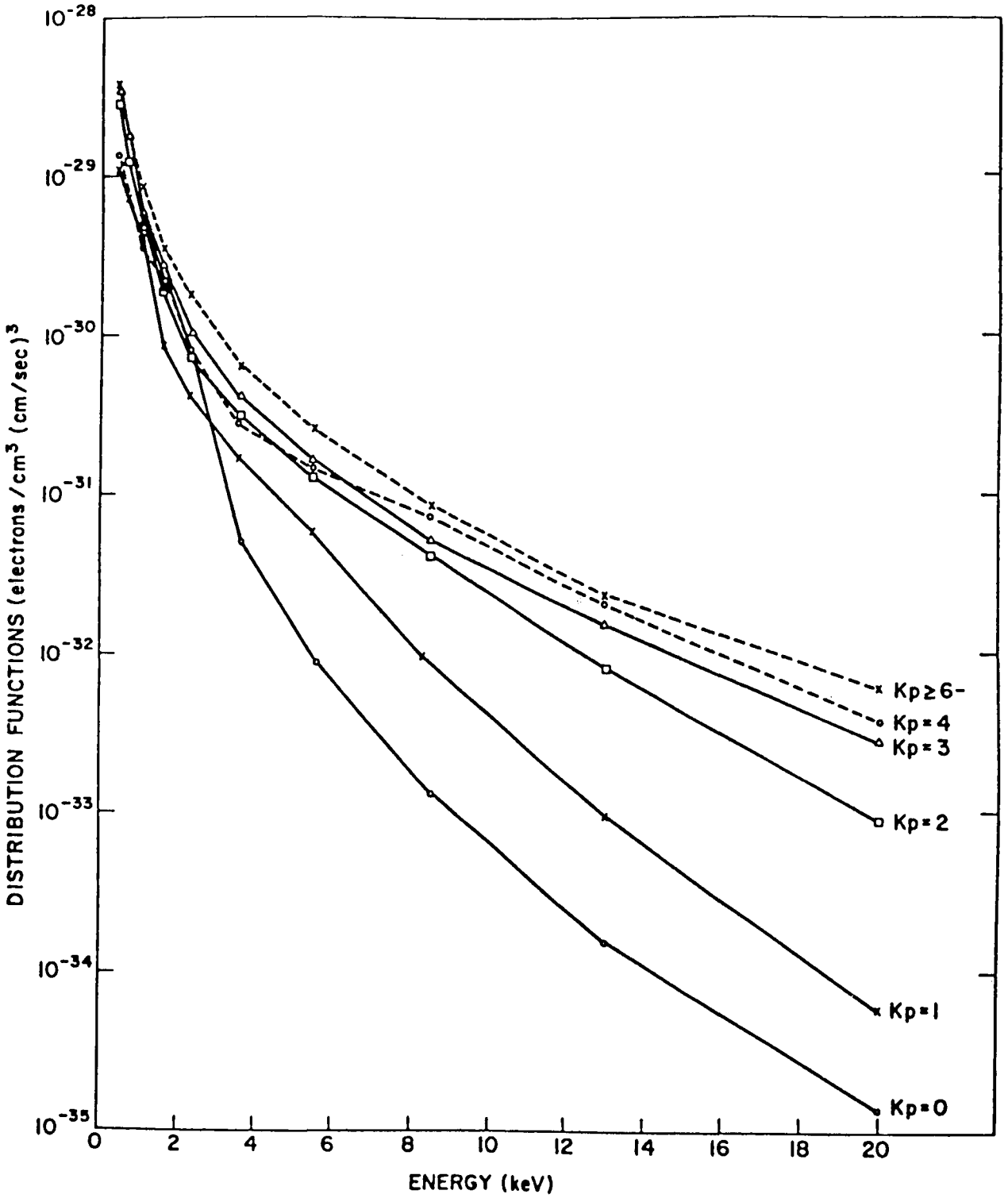

Figure 4. The average distribution function at the pre-noon average energy maximum for each K_p level. The logarithm of the distribution function is plotted versus energy on a linear scale. Only points at energies above 440 eV are included [from Hardy et al., 1985].

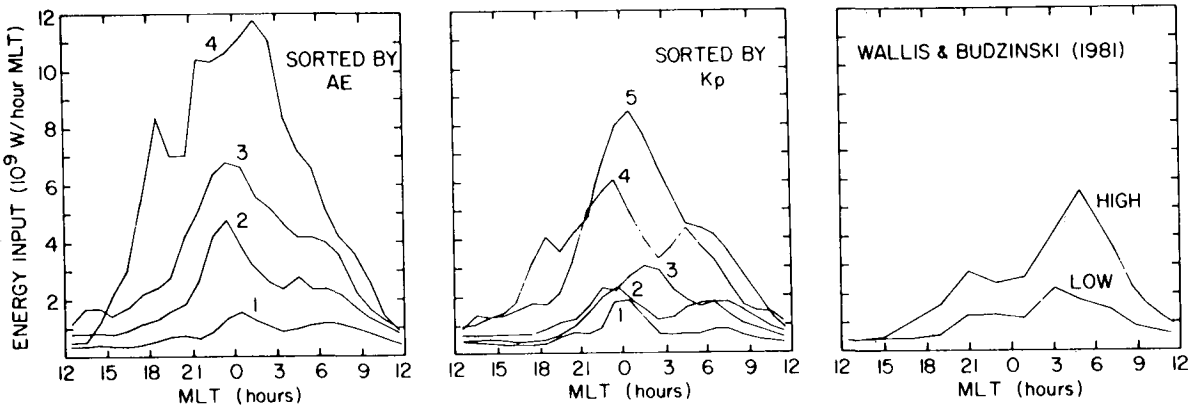

Figure 5. Total precipitating electron energy input (both hemispheres) per hour magnetic local time.(a) Data sorted according to AE index, (b) data sorted according to Kp index, and (c) results calculated from data given in Tables A1 and A2 of Wallis and Budzinski [1981].